

First-Principles and Microkinetic Simulation Studies of the Structure Sensitivity of Cu Catalyst for Methanol Steam Reforming

Sha-Sha Wang,^{†,‡,#} Xiang-Kui Gu,^{‡,#} Hai-Yan Su,[†] and Wei-Xue Li^{*,†,§,||}

[†]State Key Laboratory of Catalysis, State Key Laboratory of Molecular Reaction Dynamics, Dalian Institute of Chemical Physics, Chinese Academy of Sciences, Dalian 110623, China

[‡]Department of Chemical Engineering and Materials Science, Wayne State University, Detroit, Michigan 48202, United States

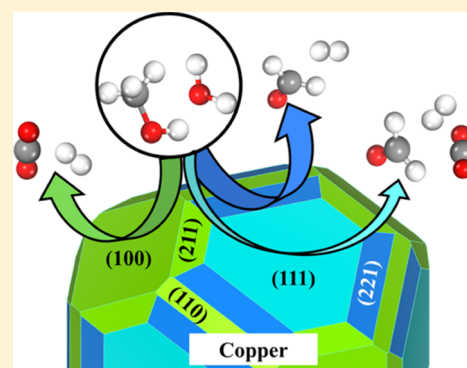
[§]Department of Chemical Physics, School of Chemistry and Materials Science, iChEM, University of Science and Technology of China, Hefei 230026, China

^{||}CAS Excellence Center for Nanoscience, Hefei National Laboratory for Physical Sciences at Microscale, Hefei 230026, China

[‡]University of Chinese Academy of Sciences, Shijingshan District, Beijing 100049, China

S Supporting Information

ABSTRACT: High CO₂ and H₂ selectivity are important issues for methanol steam reforming (MSR) to provide H₂ as a clean energy carrier. The structure sensitivity and the factors governing the activity and selectivity for MSR on Cu catalysts are systematically investigated using density functional theory calculations and microkinetic simulation. Potential energy surfaces including water dissociation, methanol dehydrogenation, formaldehyde desorption and coupling with oxygen-containing intermediates, and formation of hydrogen and carbon dioxide are calculated over Cu(111), (100), (221), (211), and (110) surfaces, respectively. It is found that Cu(110) facet is the most active and selective toward carbon dioxide; Cu(221) is also active but highly selective toward formaldehyde, whereas Cu(111) is nearly inactive. Degree of rate control analysis shows that the activity is controlled mainly by methanol dehydrogenation to formaldehyde, whereas the degree of selectivity control shows that the selectivity toward formaldehyde or carbon dioxide depends sensitively on competition between formaldehyde desorption and coupling with surface oxygen. For Cu(110), abundance of both methoxy and oxygen as well as available vacant sites key for its high activity and selectivity toward carbon dioxide, whereas lack of oxygen on Cu(221) makes the corresponding surface highly selective for formaldehyde. The present work highlights the great influence of Cu surface orientations on the activity and selectivity for MSR.



1. INTRODUCTION

Hydrogen production from methanol has attracted considerable interest in providing fuel for polymer electrolyte membrane fuel cells^{1–3} because of its benefits of low cost, liquid offering, safe storage, and high H/C ratio.⁴ Among the transformations of methanol, such as methanol decomposition, methanol partial oxidation, and methanol steam reforming (MSR, CH₃OH + H₂O → CO₂ + 3H₂), MSR is a promising process with high selectivities towards CO₂ and H₂.³ To understand the underlying factors that govern the reactivity, the mechanisms of MSR have been studied widely. Various reaction pathways have been proposed, including the CO-mediated pathway, where methanol completely dehydrogenates to CO followed by the water gas shift reaction (WGS), the pathways via methyl formate, and the pathways via formaldehyde intermediate.^{5–11} Among these, the methyl formate pathway is reported to be less favorable,¹² and the CO₂ selectivity in the CO-mediated pathway is affected by the reverse WGS.¹³ The formaldehyde pathway is suggested to be more favorable in providing high CO₂ selectivity,^{10,14} and it is generally composed

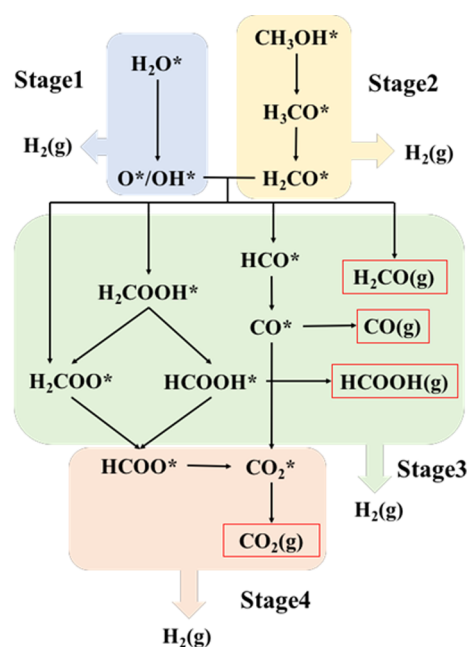
of four stages as shown in Scheme 1. Stages 1 and 2 involve H₂O dissociation and CH₃OH partial decomposition to CH₂O. In stage 3, CH₂O formed can further dehydrogenate to CO or couple with OH/O from H₂O dissociation to produce H₂COOH/H₂COO intermediate, which can sequentially dehydrogenate to CO₂ (stage 4). In this pathway, it is clear that the high selectivity of CO₂ is controlled by stage 3.

Cu-based catalysts (i.e., Cu/ZnO/Al₂O₃) are commonly used for MSR because of their superior selectivity toward CO₂, but suffer from thermal instability, such as pyrophoricity, sintering, and deactivation.^{3,15} Though identification of the active sites under reaction condition remains a long-standing challenge in heterogeneous catalysis, it is generally suggested that the active component of this type of catalyst is metallic Cu,^{3,16} and the oxidation of Cu can significantly decrease the activity for MSR.¹⁶ Recently, noble metal-based catalysts have also been

Received: January 3, 2018

Revised: March 13, 2018

Published: April 26, 2018

Scheme 1. Reaction Network of MSR via CH₂O Intermediate

reported for this process, such as α -MoC supported Pt⁴ and intermetallic compounds (i.e., PdZn, PtZn, and PdIn),^{17–21} which exhibit good activity, stability, and high CO₂ selectivity. To improve the atomic efficiency of the noble metals, ZnO-supported single-atom catalysts are also reported to be promising for MSR.²² In general, the catalysts used for this process are supported nanoparticles, and various surface facets can be exposed depending on the supports and the reactant atmosphere.²³ Consequently, the structure sensitivity will have a significant effect on the reactivity of this process. This is supported by the reports for the related methanol decomposition process on Cu catalysts. For C–H bond breaking of CH₃O (rate-limiting step), as an example, it is found that Cu(110), Cu(100), and Cu clusters exhibit lower barriers than Cu(111).^{24–26} On the other hand, CH₃OH tends to break C–H bond first on small Cu₄ clusters for CH₃OH decomposition, which is different from the decomposition pathway via O–H bond scission first on Cu surfaces.²⁷ Although many efforts have been reported for the structure sensitivity of CH₃OH decomposition, only a limited understanding of this effect on MSR exists.

In this work, the structure sensitivity for MSR via the most favorable CH₂O-mediated pathway is systematically studied by means of density functional theory (DFT) calculations combined with the microkinetic simulations on various metallic Cu surfaces. The remaining paper is organized as follows: In section 2, Computational setup for DFT and microkinetic simulation are described in detail. Then, the Results and Discussion are reported in section 3. We first report possible Cu surfaces exposed via Wulff construction based on DFT calculations, in addition to the available experimental data. After this, the key results of the potential energy surfaces for MSR including dehydrogenation of water and methanol, formaldehyde desorption and coupling with surface oxygen, and so forth on various Cu surfaces are given. The resulting energetics and barriers are input as parameters into the microkinetic simulation, from which the corresponding activity

and selectivity toward carbon dioxide can be derived. The key issues to determine the activity and selectivity as well as dependence on surface orientation will be analyzed via degree of rate control (DRC) and selectivity control, respectively. A brief summary is given finally.

2. COMPUTATIONAL METHODS

2.1. DFT Calculations. DFT calculations were performed using Vienna Ab initio Simulation Package. The exchange correlation interaction is described by the generalized gradient approximation²⁸ and Perdew–Burke–Ernzerhof (PBE)²⁹ functional with the consideration of van der Waals interaction (optPBE–vdW).^{30,31} The Kohn–Sham equations are solved using a plane wave basis set with a kinetic energy cutoff of 400 eV. The optimized lattice constant of bulk Cu is 3.64 Å, in agreement with the experimental value of 3.62 Å.³² Although the model of the Cu nanoparticle would be realistic to study the structure sensitivity, it remains formidable to explore complex reaction network such as MSR for the current DFT simulations. Alternatively, the nanoparticle is divided by the most exposed facets based on Wulff construction and experimental reports,²³ such as Cu(111), Cu(100), Cu(110), Cu(211), and Cu(221). These surfaces are modeled using relatively simple slab models. To keep a similar super cell volume in each model, Cu(111) and Cu(100) with (3 × 3) unit cells involve four and five layers, respectively, whereas Cu(110) involves seven layers with a (2 × 3) unit cell. In the case of the stepped Cu(221) and Cu(211), four-layer slabs are used in (111) direction with (3 × 1) and (1 × 3) unit cells, respectively. A (5 × 5 × 1) *k*-point mesh is used to sample the surface Brillouin zone,³³ and a 15 Å vacuum is introduced with the correction of dipole moment between the repeated slabs along the *z*-direction. During optimization, half of the bottom layers of the slabs are fixed, whereas the remaining atoms and adsorbates are relaxed until the residual force is less than 0.02 eV/Å.

Wulff construction of Cu is based on the surface energies of various surfaces, E_s , which is determined by

$$E_s = (E_{\text{slab}} - N \times E_{\text{bulk}}) / 2A \quad (1)$$

where E_{slab} and E_{bulk} are the total energies of the slab and the bulk Cu atom, respectively. N and A are the number of Cu atoms in the slab and the slab surface area, respectively. Adsorption energies (E_{ad}) of the adsorbates are calculated by

$$E_{\text{ad}} = E_{\text{ads/sub}} - E_{\text{ads}} - E_{\text{sub}} \quad (2)$$

where $E_{\text{ads/sub}}$, E_{sub} , and E_{ads} are the total energies of the optimized adsorbate–substrate system, the clean substrate, and the gas-phase adsorbate, respectively. Transition state of the elementary step is located by the climbing-image nudged elastic band^{34,35} and the advanced force reversed methods.³⁶

2.2. Microkinetic Simulations. The forward and backward rate constants of the elementary steps are calculated using eq 3

$$k = \frac{k_B T}{h} \frac{Q^{\text{TS}}}{Q} e^{-E_a/k_B T} \quad (3)$$

where k_B , T , h , E_a , Q^{TS} , and Q are the Boltzmann constant, temperature, Planck's constant, activation barrier, partition function of the transition state, and partition function of the initial state, respectively. Partition function is the summation of all possible states including translation, rotation, and vibration modes. For surface reactions, vibrational degree of freedom becomes dominating, and the corresponding pre-exponential

factor is mainly governed by the $k_B T/h$ term. In present work, it is set to 10^{13} s^{-1} for all elementary steps considered. The rate of molecular adsorption is determined by the rate of surface impingement of gas-phase molecules. The flux of the incident molecule is given by Hertz–Knudsen equation³⁷

$$F = \frac{P}{\sqrt{2\pi m k_B T}} \quad (4)$$

The molecular adsorption rate constant is expressed as

$$k_{\text{ads}} = -\frac{PA'}{\sqrt{2\pi m k_B T}} S \quad (5)$$

where P is the partial pressure of the molecule, S is the sticking coefficient which is assumed to be 1.0, A' is the surface area, and m is the mass of the molecule. In the case of desorption process, we assume that there are three rotational degrees of freedom and two translational degrees of freedom in the transition state. The desorption rate constant is calculated as

$$k_{\text{des}} = \frac{k_B T^3}{h^3} \frac{A'(2\pi k_B)}{\sigma \theta_{\text{rot}}} e^{-E_{\text{des}}/k_B T} \quad (6)$$

where σ and θ_{rot} are the symmetry number and the rotational temperature of the species,³⁸ respectively, and the values used here are shown in Table S1.

Microkinetic simulations are performed by the MKMCXX program, and the details can be found elsewhere.^{39,40} For MSR, the gas phase contains a mixture of H_2O and CH_3OH in a 2:1 molar ratio at a total pressure of 1 atm. The control of the elementary step in the activity is analyzed by the “DRC” method developed by Campbell et al.^{41–43} For the elementary step i , the DRC, $X_{\text{RC},i}$ can be defined as

$$X_{\text{RC},i} = \frac{k_i}{r} \left(\frac{\partial r}{\partial k_i} \right)_{k_j \neq i, K_i} = \left(\frac{\partial \ln r}{\partial \ln k_i} \right)_{k_j \neq i, K_i} \quad (7)$$

where k_i , K_i , and r are the rate constant, the equilibrium constant for elementary step i , and the reaction rate, respectively. Furthermore, the DRC coefficients have to obey the sum rule over all elementary steps in the mechanism

$$\sum_i X_{\text{RC},i} = 1 \quad (8)$$

The degree of selectivity control (DSC) is also performed,⁴⁴ which quantifies the particular elementary step that influences the selectivity to certain products. DSC for a particular key component is defined in the following manner

$$\varepsilon_{c,i} = \left(\frac{\partial \eta_c}{\partial k_i/k_i} \right)_{k_j \neq i, K_i} = \left(\frac{\partial \eta_c}{\partial \ln(k_i)} \right)_{k_j \neq i, K_i} \quad (9)$$

where $\varepsilon_{c,i}$ is the DSC of product c because of a change in the kinetics of the elementary step i and η_c is the selectivity of a key product component. The products of MSR considered in the present study are CO_2 , CO , CH_2O , HCOOH , and H_2 .

3. RESULTS AND DISCUSSION

3.1. Wulff Construction. The calculated surface energies of a series of possible Cu surfaces are shown in Table 1. On the basis of these energetics, the morphology and proportions of the exposed surfaces for free standing Cu catalysts can be obtained using Wulff construction (Figure 1). We find that the

Table 1. Calculated Surface Energies (E_s) of Various Cu Surfaces and the Surface Area Proportion (S_s) of the Surfaces Exposed on a Free Standing Cu Particle from Wulff Construction

surface	$E_s/\text{meV}/\text{\AA}^2$ (J/m^2)	S_s (%)
(111)	81.82 (1.31)	41
(100)	90.66 (1.45)	21
(221)	90.15 (1.44)	20
(211)	92.24 (1.48)	6
(311)	94.34 (1.51)	12
(110)	96.67 (1.55)	
(301)	99.81 (1.60)	
(302)	101.05 (1.62)	
(210)	103.46 (1.66)	

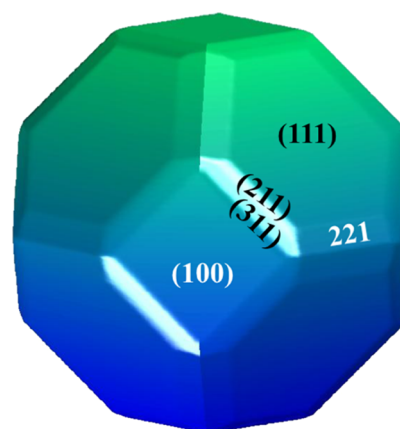


Figure 1. Morphology of a free-standing Cu catalyst from Wulff construction based on the calculated surface energies.

mainly exposed surfaces include Cu(111), Cu(100), Cu(221), Cu(211), and Cu(311). Among these, the closely packed (111) surface exhibits the highest proportion of 41% because of its lowest surface energy ($81.82 \text{ meV}/\text{\AA}^2$). The comparable surface energies of 90.66 and $90.15 \text{ meV}/\text{\AA}^2$ for (100) and (221) result in a similar exposed proportion ($\sim 20\%$). The remaining exposed surfaces with a proportion of 18% are the stepped (211) and (311), and only the (211) surface is considered in the present work because of their similar configurations. The less exposure of Cu(211) with a lower surface energy than Cu(311) is compensated by the most exposed Cu(111), which is adjacent to Cu(211). We note that the morphology derived is constructed based on surface energy without considering the influence of the reaction conditions. Actually, when there is water present in the gas environment, a considerable amount of Cu(110) is exposed.^{23,45} Thus, this surface is also considered below. In the following, to identify the structure sensitivity of MSR on the Cu catalyst, the energetics associated with the elementary steps involved in the reaction network of this process are systematically investigated, and only the most favorable CH_2O -mediated pathway is considered (Scheme 1), as mentioned above.

3.2. Water Dissociation. The facile water adsorption and dissociation are critical to provide OH^*/O^* as the oxidant for MSR, which can further react with the intermediates from CH_3OH decomposition to give a high CO_2 selectivity. Water monomer prefers to bind to the top site of the surface Cu atoms (Figure S1), and the calculated binding energy becomes gradually stronger from -0.34 to -0.56 eV when the surface

varies from Cu(111) to (100), (110), (211), and (221) (Table 2). The strongest binding strengths on the stepped Cu(211)

Table 2. Adsorption Energies (eV) of Intermediates Involved in MSR on Cu Surfaces

species	Cu(111)	Cu(100)	Cu(221)	Cu(211)	Cu(110)
CH ₃ OH	-0.50	-0.56	-0.75	-0.73	-0.65
CH ₃ O	-2.78	-2.81	-2.95	-2.81	-2.85
CH ₂ O	-0.42	-0.67	-0.65	-0.60	-0.68
HCO	-1.59	-1.73	-1.89	-1.79	-1.83
H ₂ COOH	-2.67	-2.85	-3.02	-2.99	-2.99
H ₂ COO	-4.60	-5.20	-4.64	-5.08	-5.37
HCOOH	-0.50	-0.57	-0.75	-0.70	-0.67
HCOO	-3.23	-3.34	-3.69	-3.54	-3.51
H ₂ O	-0.34	-0.37	-0.56	-0.52	-0.47
OH	-3.51	-3.56	-3.72	-3.68	-3.62
CO	-0.92	-0.89	-0.96	-0.90	-0.90
CO ₂	-0.19	-0.20	-0.24	-0.21	-0.22
O	-1.97	-2.25	-2.10	-1.99	-1.91
H	-0.18	-0.05	-0.20	-0.17	-0.04

^aWe note that the data for Cu(111) are adopted from ref 11.

and Cu(221) suggest that water tends to enrich at the defective steps. For water dissociation to OH* and H*, it is found that Cu(111) exhibits the highest barrier of 1.18 eV, slightly lower than the reported values of 1.24–1.36 eV^{10,46–48} because of the vdW interaction considered here. The more favorable dissociation of water is observed on the more open and stepped surfaces with the calculated barriers of ~0.83 eV (Table 3). The lower barriers come from the fact that the surface Cu atoms on these surfaces have a lower coordination number as compared to that on Cu(111), resulting in stronger binding energies of OH species. In the case of OH* dissociation to O* and H*, we find this process is very difficult to occur on all surfaces studied because of the much high dissociation barriers (>1.53 eV) and high endothermicities (>0.45 eV), whereas the disproportionation of two OH* to form H₂O* and O* is much more favorable as compared to

OH direct dissociation (Table 3), in particular on Cu(111) (0.77 eV) and Cu(100) (0.72 eV). These suggest that the oxidants for MSR on the Cu catalyst might be the coexisting OH* and O*. From Figure S2a, it is clear that Cu(111) exhibits the lowest activity for water dissociation, whereas the stepped Cu(221) and Cu(211) exhibit the highest activity in comparison to the other surfaces.

3.3. CH₃OH Dehydrogenation to CH₂O. Similar to water adsorption, the binding energy of CH₃OH on the top of surface Cu atoms also becomes gradually stronger from -0.50 to -0.75 eV as the surface changes from Cu(111) to (100), (110), (211), and (221). For CH₃OH dehydrogenation to CH₃O*, we find that CH₃OH tends to break the O–H bond first followed by the scission of C–H bond, consistent with the reported theoretical and experimental observations.^{25,26,49–54} The calculated barrier of 1.07 eV for O–H bond cleavage on Cu(111) is at least 0.26 eV higher than that on the other surfaces. This is because the O–H bond distance of 1.42 Å in the transition state on Cu(111) is shorter than that on the other surfaces (Table S2), where the O–H bond is more activated. In the case of C–H bond scission of CH₃O* to form CH₂O*, we find that the perpendicular CH₃O* tilts first with one C–H bond pointing to the surface. The process of C–H bond breaking is highly endothermic by at least 0.86 eV. Kinetically, Cu(111) and Cu(100) exhibit the highest activation barriers of 1.33 and 1.39 eV, respectively. The barrier can decrease to be 1.04 and 1.09 eV on the stepped Cu(221) and Cu(211) because these surfaces facilitate the tilt of CH₃O*. Figure S2b indicates that the stepped surfaces show the highest activity for CH₂O* formation from CH₃OH* dehydrogenation, whereas Cu(111) has the lowest activity with higher barriers for O–H and C–H bond cleavages.

3.4. Competitive Reactions toward Selectivity. Once CH₂O* and OH*/O* intermediates are produced, three competitive pathways can occur, including CH₂O* coupling with OH*/O* to form H₂COOH*/H₂COO* intermediate, CH₂O* dehydrogenation to CO*, and CH₂O* desorption. These processes are crucial for the selectivities of CO₂, HCOOH, CO, and CH₂O in MSR. We find that the

Table 3. Activation Barriers (E_a, eV) and Reaction Energies (E_r, eV) of the Elementary Steps Involved in MSR on Cu Surfaces

elementary step	Cu(111)		Cu(100)		Cu(221)		Cu(211)		Cu(110)	
	E _a	E _r								
(1) H ₂ O* + * → OH* + H*	1.18	-0.14	0.84	-0.02	0.83	-0.15	0.80	-0.11	0.83	0.03
(2) OH* + * → O* + H*	1.70	0.60	1.68	0.45	1.54	0.67	1.53	0.76	1.58	0.90
(3) OH* + OH* → H ₂ O* + O*	0.77	0.74	0.72	0.52	1.39	0.81	1.14	0.87	0.95	0.88
(4) CH ₃ OH* + * → CH ₃ O* + H*	1.07	-0.18	0.76	-0.02	0.81	-0.10	0.75	0.03	0.80	0.05
(5) CH ₃ O* + * → CH ₂ O* + H*	1.33	0.99	1.39	0.90	1.04	0.91	1.09	0.86	1.18	0.95
(6) OH* + CH ₂ O* → H ₂ COOH* + *	0.38	-0.39	0.45	-0.27	0.15	-0.30	0.19	-0.37	0.02	-0.35
(7) H ₂ COOH* + * → HCOOH + H*	0.92	0.07	0.81	0.30	1.00	0.15	0.87	0.20	0.80	0.36
(8) HCOOH* + * → HCOO* + H*	0.53	-0.51	0.52	-0.42	0.65	-0.75	0.61	-0.61	0.59	-0.49
(9) H ₂ COOH* + * → H ₂ COO + H*	1.20	0.21	0.96	-0.01	1.64	0.57	1.34	0.13	1.21	-0.02
(10) H ₂ COO* + * → HCOO* + H*	0.81	-0.65	0.81	-0.11	0.57	-1.17	1.09	-0.55	0.99	-0.10
(11) CH ₂ O* + * → HCO* + H*	0.83	0.31	0.94	0.54	0.79	0.21	0.87	0.29	0.70	0.46
(12) HCO* + * → CO* + H*	0.29	-0.76	0.29	-0.46	0.46	-0.52	0.43	-0.53	0.50	-0.35
(13) O* + CH ₂ O* → H ₂ COO* + *	0.24	-0.79	0.43	-0.79	0.48	-0.40	0.38	-1.00	0.19	-1.28
(14) H ₂ COO* + O* → HCOO* + OH*	1.12	-1.25	1.35	-0.60	0.77	-1.83	1.44	-1.30	0.78	-1.01
(15) CO* + O* → CO ₂ * + *	0.71	-0.47	0.82	-0.23	0.67	-0.35	0.76	-0.49	0.17	-0.57
(16) HCOO* + * → CO ₂ * + H*	1.26	0.51	1.27	0.74	1.55	0.91	1.45	0.82	1.39	0.91
(17) HCOO* + O* → CO ₂ * + OH*	1.09	-0.09	1.00	0.25	1.40	0.24	1.41	0.06	1.61	0.01

^aWe note that part of the data on Cu(111) are adopted from ref 11.

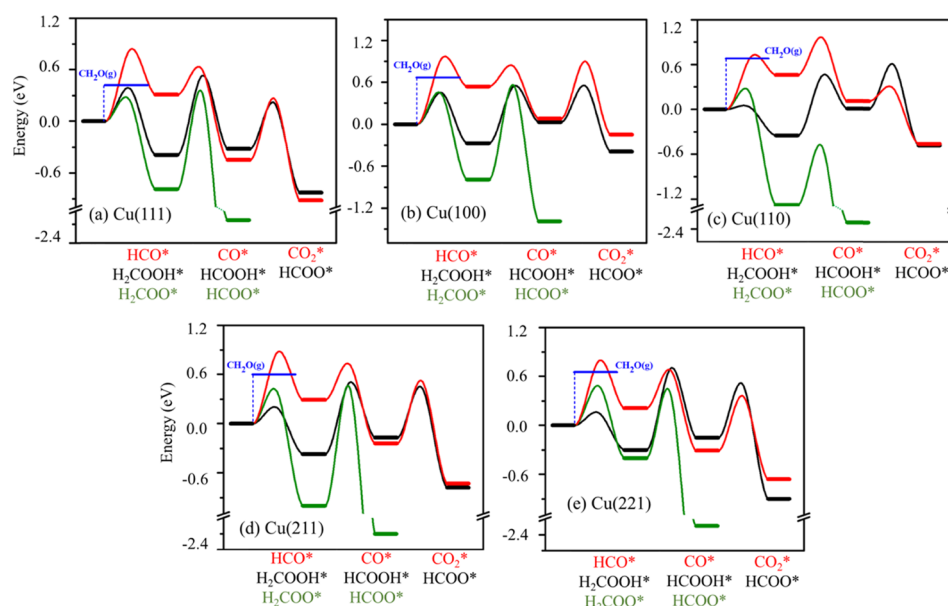


Figure 2. Energy profiles for the formaldehyde reaction on Cu(111) (a), Cu(100) (b), Cu(110) (c), Cu(211) (d), and Cu(221) (e). Reaction starts from a common energy reference $\text{CH}_2\text{O}^* + \text{O}^* + \text{OH}^*$, and four competitive reaction pathways are considered: (1) CH_2O^* desorption (blue), (2) CH_2O^* dehydrogenation to CO^* followed by CO^* reaction with O^* to CO_2^* (red), (3) CH_2O^* reaction with O^* to form H_2COO^* followed by its dehydrogenation to HCOO^* (green), and (4) CH_2O^* reaction with OH^* to form H_2COOH^* followed by its dehydrogenation to CO_2^* (in black).

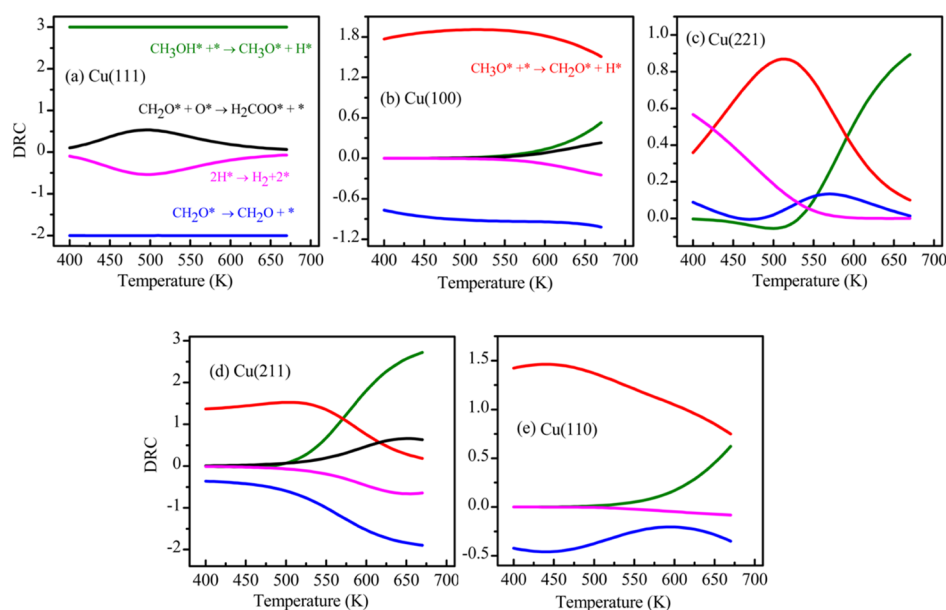


Figure 3. DRC of the elementary steps for CO_2 formation on Cu(111) (a), Cu(100) (b), Cu(221) (c), Cu(211) (d), and Cu(110) (e) as a function of temperature.

dehydrogenation of CH_2O^* to CO^* on all these surfaces are less favorable with much higher barriers as compared to its desorption and coupling processes (Table 3 and Figure 2). This suggests that the CO selectivity for MSR on Cu-based catalysts should be very low, consistent with the experiments on Cu/ Al_2O_3 .⁵⁵ On the other hand, the desorption of CH_2O^* into gas phase is less favorable on all these surfaces than CH_2O^* coupling with OH^*/O^* . In the case of the coupling reaction, CH_2O^* reaction with OH^* to form H_2COOH^* on Cu(111) and (100) exhibits slightly higher barriers than its reaction with O^* to form H_2COO^* , whereas on the other surfaces, H_2COOH^* formation is kinetically less facile than that of

H_2COO^* . To produce CO_2 , H_2COO^* and H_2COOH^* tend to dehydrogenate to HCOO^* first. In the case of H_2COOH^* dehydrogenation, we find that the C–H bond scission exhibits lower barriers than O–H bond scission (Table 3). Moreover, the H_2COO^* formation on all surfaces is much more favorable energetically, resulting in the overall barriers of HCOO^* formation via CH_2O^* reaction with O^* being lower on all surfaces (Figure 2).

3.5. HCOO Decomposition to CO_2 . At the last stage, the most stable bidentate HCOO^* tends to transform to the less stable monodentate geometry to facilitate the C–H bond scission and release CO_2 . It is found that Cu(111) and Cu(100)

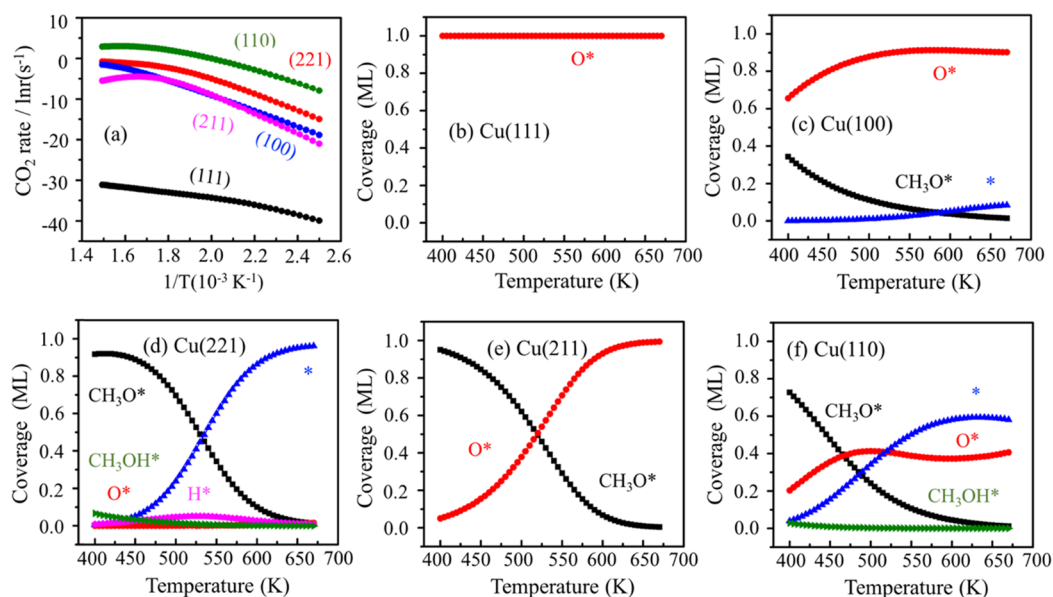


Figure 4. Activity trend of CO₂ formation (a) and the coverages of the most abundant species (black for methoxy, red for oxygen, blue for vacant sites, purple for hydrogen, and green for methanol) for MSR on Cu(111) (b), Cu(100) (c), Cu(221) (d), Cu(211) (e), and Cu(110) (f) as a function of temperature.

exhibit lowest barriers of ~ 1.26 eV (Figure S3), similar to the reported value of 1.30 eV on Cu(111).^{24,56,57} On the other surfaces, the barriers are slightly higher with the values of 1.39–1.55 eV, consistent with the experimental result of 145.2 ± 7.2 kJ/mol on Cu(110).^{58,59} This is because of the stronger binding of HCOO* on these surfaces as compared to that on Cu(111) and (100). Thermodynamically, this process is endothermic on all surfaces considered (Table 3). We note that desorption of H₂ is very facile on these surfaces because of the weaker dissociative binding of hydrogen, as shown in Table 2.

3.6. Microkinetic Simulations. On the basis of the above results, the microkinetic simulations are performed to obtain insights into the trends of activity and selectivity of these surfaces for MSR, which can guide the design of Cu-based catalysts with optimal reactivity for this reaction. Furthermore, the DRC and DSR analyses as a function of temperature are also performed to understand the importance of the elementary steps to activity and selectivity. We note that the positive values of DRC/DSC for a particular step means that this step is a limiting step, and the decrease in the barrier facilitates to increase the activity/selectivity. Whereas the negative values indicate the inhibitive step, the decrease of its barrier will lower the activity/selectivity. Here, we only show the steps with the absolute values of DRC/DSC higher than 0.01. On the basis of CO₂ formation, Figure 3a clearly shows that on Cu(111), the activity is mostly determined by CH₃OH* decomposition to CH₃O* at 400–675 K. This might be because the facile desorption of CH₃OH* on Cu(111) would limit its dehydrogenation because of its weak binding. Moreover, it is found that the coupling reaction between CH₂O* and O* is also important to control the activity of MSR on Cu(111) at ~ 450 –550 K. On Cu(110) and (100), the activity is mostly controlled by CH₃O* dehydrogenation to CH₂O*, and the importance of this step significantly decreases at higher temperatures (Figure 3e,b). This is because the increase of the importance for CH₃OH* decomposition to CH₃O* due to CH₃OH* desorption becoming more favorable at higher temperatures. On the stepped Cu(211) and (221), the

importance of the elementary step for the activity is highly temperature-dependent (Figure 3d,c). It is generally found that CH₃O* dehydrogenation to CH₂O* is the most important at temperatures lower than ~ 575 K, whereas CH₃OH* decomposition to CH₃O* becomes the most important at higher temperatures.

These findings clearly show that the activity of MSR is controlled by CH₃O* dehydrogenation to CH₂O* on majority of the surfaces considered, consistent with the literature where this step is suggested to be the rate-limiting step for MSR on Cu-based catalysts.³ In addition, it is found that the desorption of CH₂O* has the most negative effect on the CO₂ formation on these surfaces except for Cu(211), suggesting that prohibition of this desorption facilitates the formation of CO₂. This is understandable with the consideration that CH₂O* desorption will decrease the probability of CH₂O* coupling reactions, limiting the CO₂ formation consequently.

The above results indicate that the steps involving CH₃O* are very important for MSR, and the abundance of CH₃O* on the surface is crucial to provide CH₂O* coupling with the oxidants OH*/O* (the coverage of CH₂O* would be very low due to the facile coupling reactions). On the other hand, we find the coverage of O* is much higher than OH*, suggesting that O* is the oxidant for MSR and its abundance on the surface is also critical. Furthermore, the abundance of the vacant site (*) facilitates to avoid the poisoning of the surface and provides the sites for the consecutive reactions. Thus, the surface providing the optimal coverage distributions of CH₃O*, O*, and the vacant site would exhibit a high activity for MSR. Figure 4a shows that Cu(110) exhibits the highest activity for CO₂ formation, whereas Cu(111) exhibits the lowest one. This is because Cu(110) provides considerable coverage distributions for all these three species (Figure 4f), whereas Cu(111) is prone to be poisoned by the almost fully covered O* (Figure 4b). In the case of the other surfaces, CH₃O* and the vacant site are the most abundant on Cu(221) because the O* formation is limited by the high barrier of OH* disproportionation (Figure 4d), whereas CH₃O* and O* are the most

abundant on Cu(100) and Cu(211) (Figure 4c,e). The limited coverages of O* on Cu(221) and the vacant site on Cu(100) and Cu(211) result in lower activity for CO₂ formation on these surfaces as compared to Cu(110).

In the case of selectivity, we find that the selectivities of the side-products CO and HCOOH are significantly lower as compared to that of CO₂, CH₂O, and H₂. On Cu(221), the CH₂O and H₂ selectivity are dominant with a ratio of 1:1 at the studied temperature range of 450–650 K because there is limited oxidant O* on this surface to couple with CH₂O*, as discussed above. This implies that Cu(211) does not work for MSR, and the products are from the decomposition of CH₃OH. On the other surfaces, the selectivities of CO₂ and CH₂O are highly temperature-dependent. Figure 5 clearly

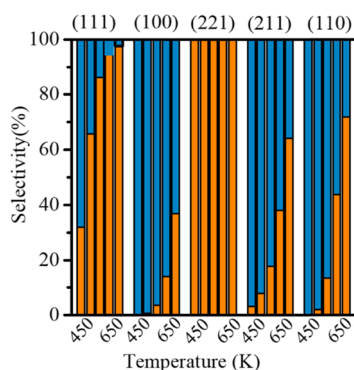


Figure 5. CO₂ (blue) and CH₂O (orange) selectivity for MSR on Cu surfaces as a function of temperature.

shows that the CO₂ selectivity decreases with an increase in the temperature, whereas the opposite trend is observed for CH₂O selectivity. These result in the selectivity of CH₂O being higher than that of CO₂ when the temperature is higher than ~500 K on Cu(111) and ~600 K on Cu(211) and Cu(110). The trend variation of formaldehyde selectivity on temperature is consistent with experimental finding on the Cu foil.⁶⁰ This is because desorption of CH₂O is improved by the high temperature. At a typical temperature of ~523 K for MSR, the main products are CO₂ and H₂ with a ratio of ~1:3 on Cu(110), (100), and (211). However, the CH₂O and H₂ products are dominant on Cu(111), similar to that on Cu(221). The degree selectivity control analysis shows that on Cu(111), (100), and (211), the selectivity of CO₂ for MSR is mainly positively and negatively affected by the coupling reaction of CH₂O* with O* and the desorption of CH₂O*, respectively (Figure 6). These suggest that lowering the barrier of the coupling reaction and increasing the barrier of CH₂O* desorption would improve the CO₂ selectivity, whereas the opposite trend is observed for CH₂O selectivity on these surfaces. On Cu(110), the selectivity seems to be controlled by multiple steps. Besides these two steps, the dehydrogenation of CH₃OH*, CH₃O*, and H₂COO* as well as H₂ desorption are also important.

On the basis of intrinsic activity and selectivity of individual facets studied above, it is interesting to discuss the overall activity and selectivity of Cu particles. First of all, we assume that Cu particles follow exactly the same morphology from the Wulff construction (Figure 1). We note that though the Cu(111) facet is the most abundant, its reactivity is too low to contribute to the overall activity and selectivity. Whereas the surface areas of Cu(221), (211) and (100) are close, their

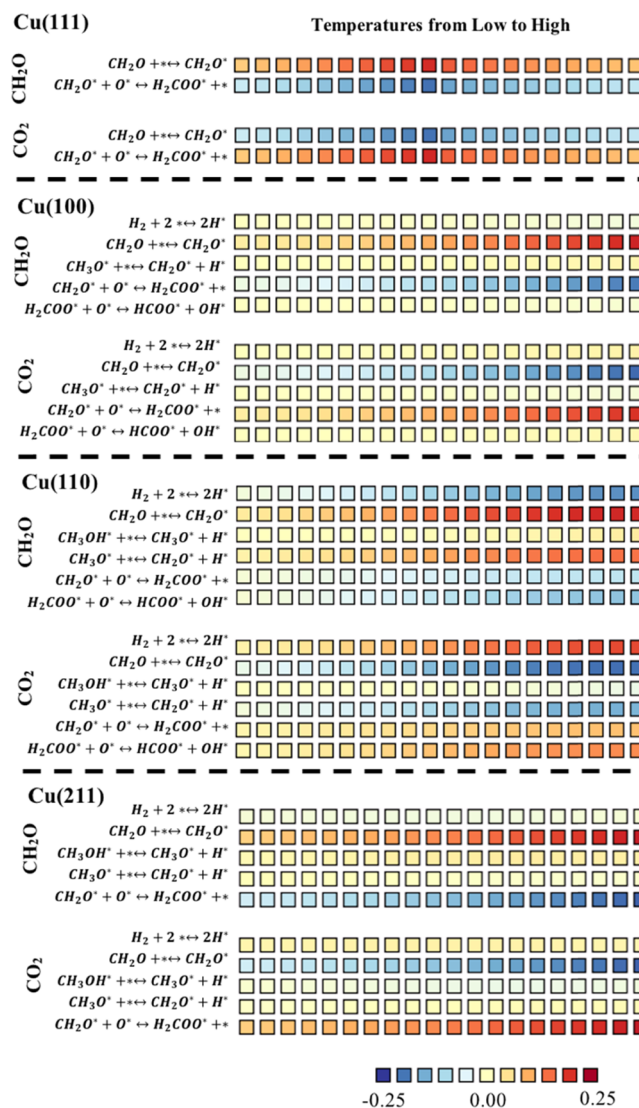


Figure 6. DSC of the elementary step for CO₂ and CH₂O formation on Cu surfaces as a function of temperature.

intrinsic activity and selectivity determine therefore the overall reactivity. As shown in Figure 4a, Cu(221) is much more active than Cu(211) and Cu(100) over the wide range of temperature, in particular at low temperature, and its selectivity would therefore decide the overall selectivity. This implies that Cu catalysts with the corresponding morphology will be highly selective to formaldehyde. Second, when there is water present in the gas environment,²³ Cu(110) would be exposed at the expense of Cu(221). This is because Cu(110) is not only more active than Cu(221) but also highly selective toward carbon dioxide rather than formaldehyde, it can be inferred that the corresponding catalyst would become more active and selective to carbon dioxide. In other words, the presence of water would change completely the activity and selectivity of MSR over the copper catalyst. This corroborates nicely with general findings in experiments that supported Cu particles are good catalysts for MSR with high selectivity to carbon dioxide.

4. CONCLUSIONS

DFT calculations and microkinetic simulations are performed to systematically investigate the structure sensitivity for MSR on a series of Cu surfaces including Cu(111), Cu(100),

Cu(211) and Cu(221), and Cu(110). We find that the activity and selectivity of this process are highly sensitive to the surface orientations: Cu(110) is the most active and selective toward carbon dioxide; Cu(221) is active but highly selective toward formaldehyde, whereas Cu(111) is nearly inactive. Methanol dehydrogenation to formaldehyde is found to be decisive to the overall activity, whereas competition between formaldehyde desorption and coupling with surface oxygen is responsible for the selectivity toward formaldehyde or carbon dioxide, respectively. The high activity and selectivity toward carbon dioxide on Cu(110) is found to originate from the abundance of both methoxy and surface oxygen intermediates as well as available vacant sites at the same time. It is interesting to further study MSR on Cu(110) at high coverage.

■ ASSOCIATED CONTENT

Supporting Information

The Supporting Information is available free of charge on the ACS Publications website at DOI: 10.1021/acs.jpcc.8b00085.

Optimized configurations of intermediates and transition states, potential energy surfaces of water dissociation, methanol dehydrogenation to CH₂O and HCOO* decomposition to CO₂, and cartesian coordinates of the transition states on the key surfaces (PDF)

■ AUTHOR INFORMATION

Corresponding Author

*E-mail: wxli70@ustc.edu.cn.

ORCID

Hai-Yan Su: 0000-0001-9326-9647

Wei-Xue Li: 0000-0002-5043-3088

Author Contributions

#S.S.-W. and X.-K.G. contributed equally.

Notes

The authors declare no competing financial interest.

■ ACKNOWLEDGMENTS

We acknowledge funding from the National Key R&D Program of China (2017YFB0602205, 2018YFA0208603, 2017YFA0204800), the Natural Science Foundation of China (91645202, 91421315), and the Chinese Academy of Sciences (QYZDJ-SSW-SLH054, XDA09030101).

■ REFERENCES

- (1) Steele, B. C. H.; Heinzl, A. Materials for Fuel-cell Technologies. *Nature* **2001**, *414*, 345–352.
- (2) Yu, K. M. K.; Tong, W.; West, A.; Cheung, K.; Li, T.; Smith, G.; Guo, Y.; Tsang, S. C. E. Non-Syngas Direct Steam Reforming of Methanol to Hydrogen and Carbon Dioxide at Low Temperature. *Nat. Commun.* **2012**, *3*, 1230.
- (3) Palo, D. R.; Dagle, R. A.; Holladay, J. D. Methanol steam reforming for hydrogen production. *Chem. Rev.* **2007**, *107*, 3992–4021.
- (4) Lin, L.; Zhou, W.; Gao, R.; Yao, S.; Zhang, X.; Xu, W.; Zheng, S.; Jiang, Z.; Yu, Q.; Li, Y.-W.; et al. Low-Temperature Hydrogen Production from Water and Methanol using Pt/ α -MoC Catalysts. *Nature* **2017**, *544*, 80–83.
- (5) Takahashi, K.; Kobayashi, H.; Takezawa, N. On the Difference in Reaction Pathways of Steam Reforming of Methanol over Copper-Silica and Platinum-Silica Catalysts. *Chem. Lett.* **1985**, *14*, 759–762.
- (6) Peppley, B. A.; Amphlett, J. C.; Kearns, L. M.; Mann, R. F. Methanol-steam reforming on Cu/ZnO/Al₂O₃. Part 1: The reaction network. *Appl. Catal., A* **1999**, *179*, 21–29.
- (7) Peppley, B. A.; Amphlett, J. C.; Kearns, L. M.; Mann, R. F. Methanol-steam reforming on Cu/ZnO/Al₂O₃ catalysts. Part 2. A comprehensive kinetic model. *Appl. Catal., A* **1999**, *179*, 31–49.
- (8) Takezawa, N.; Iwasa, N. Steam reforming and dehydrogenation of methanol: Difference in the catalytic functions of copper and group VIII metals. *Catal. Today* **1997**, *36*, 45–56.
- (9) Lin, S.; Xie, D.; Guo, H. Pathways of Methanol Steam Reforming on PdZn and Comparison with Cu. *J. Phys. Chem. C* **2011**, *115*, 20583–20589.
- (10) Gu, X.-K.; Li, W.-X. First-Principles Study on the Origin of the Different Selectivities for Methanol Steam Reforming on Cu(111) and Pd(111). *J. Phys. Chem. C* **2010**, *114*, 21539–21547.
- (11) Wang, S.-S.; Su, H.-Y.; Gu, X.-K.; Li, W.-X. Differentiating Intrinsic Reactivity of Copper, Copper-Zinc Alloy, and Copper/Zinc Oxide Interface for Methanol Steam Reforming by First-Principles Theory. *J. Phys. Chem. C* **2017**, *121*, 21553–21559.
- (12) Lin, S.; Xie, D.; Guo, H. Methyl Formate Pathway in Methanol Steam Reforming on Copper: Density Functional Calculations. *ACS Catal.* **2011**, *1*, 1263–1271.
- (13) Jiang, C. J.; Trimm, D. L.; Wainwright, M. S.; Cant, N. W. Kinetic study of steam reforming of methanol over copper-based catalysts. *Appl. Catal., A* **1993**, *93*, 245–255.
- (14) Lin, S.; Johnson, R. S.; Smith, G. K.; Xie, D.; Guo, H. Pathways for Methanol Steam Reforming Involving Adsorbed Formaldehyde and Hydroxyl Intermediates on Cu(111): Density Functional Theory Studies. *Phys. Chem. Chem. Phys.* **2011**, *13*, 9622–9631.
- (15) Yong, S. T.; Ooi, C. W.; Chai, S. P.; Wu, X. S. Review of Methanol Reforming-Cu-based Catalysts, Surface Reaction Mechanisms, and Reaction Schemes. *Int. J. Hydrogen Energy* **2013**, *38*, 9541–9552.
- (16) Günter, M. M.; Ressler, T.; Jentoft, R. E.; Bems, B. Redox behavior of copper oxide/zinc oxide catalysts in the steam reforming of methanol studied by in situ X-ray diffraction and absorption spectroscopy. *J. Catal.* **2001**, *203*, 133–149.
- (17) Arroyo-Ramírez, L.; Chen, C.; Cargnello, M.; Murray, C. B.; Fornasiero, P.; Gorte, R. J. Supported platinum–zinc oxide core–shell nanoparticle catalysts for methanol steam reforming. *J. Mater. Chem. A* **2014**, *2*, 19509–19514.
- (18) Krajčí, M.; Tsai, A.-P.; Hafner, J. Understanding the selectivity of methanol steam reforming on the (111) surfaces of NiZn, PdZn and PtZn: Insights from DFT. *J. Catal.* **2015**, *330*, 6–18.
- (19) Rameshan, C.; Stadlmayr, W.; Weilach, C.; Penner, S.; Lorenz, H.; Hävecker, M.; Blume, R.; Rocha, T.; Teschner, D.; Knop-Gericke, A. Subsurface-Controlled CO₂ Selectivity of PdZn Near-Surface Alloys in H₂ Generation by Methanol Steam Reforming. *Angew. Chem., Int. Ed.* **2010**, *49*, 3224–3227.
- (20) Men, Y.; Kolb, G.; Zapf, R.; O’Connell, M.; Ziogas, A. Methanol steam reforming over bimetallic Pd–In/Al₂O₃ catalysts in a micro-structured reactor. *Appl. Catal., A* **2010**, *380*, 15–20.
- (21) Rameshan, C.; Lorenz, H.; Mayr, L.; Penner, S.; Zemlyanov, D.; Arrigo, R.; Hävecker, M.; Blume, R.; Knop-Gericke, A.; Schlögl, R.; Klötzer, B. CO₂-selective methanol steam reforming on In-doped Pd studied by in situ X-ray photoelectron spectroscopy. *J. Catal.* **2012**, *295*, 186–194.
- (22) Gu, X.-K.; Qiao, B.; Huang, C.-Q.; Ding, W.-C.; Sun, K.; Zhan, E.; Zhang, T.; Liu, J.; Li, W.-X. Supported Single Pt-1/Au-1 Atoms for Methanol Steam Reforming. *ACS Catal.* **2014**, *4*, 3886–3890.
- (23) Hansen, P. L.; Wagner, J. B.; Helveg, S.; Rostrup-Nielsen, J. R.; Clausen, B. S.; Topsøe, H. Atom-resolved imaging of dynamic shape changes in supported copper nanocrystals. *Science* **2002**, *295*, 2053–2055.
- (24) Mei, D.; Xu, L.; Henkelman, G. Dimer Saddle Point Searches to Determine The Reactivity of Formate on Cu(111). *J. Catal.* **2008**, *258*, 44–51.
- (25) Mei, D.; Xu, L.; Henkelman, G. Potential Energy Surface of Methanol Decomposition on Cu(110). *J. Phys. Chem. C* **2009**, *113*, 4522–4537.

- (26) Xu, L.; Mei, D.; Henkelman, G. Adaptive Kinetic Monte Carlo Simulation of Methanol Decomposition on Cu(100). *J. Chem. Phys.* **2009**, *131*, 244520.
- (27) Mehmood, F.; Greeley, J.; Zapol, P.; Curtiss, L. A. Comparative density functional study of methanol decomposition on Cu₄ and Co₄ clusters. *J. Phys. Chem. B* **2010**, *114*, 14458–14466.
- (28) Perdew, J. P.; Burke, K.; Ernzerhof, M. Generalized gradient approximation made simple. *Phys. Rev. Lett.* **1996**, *77*, 3865–3868.
- (29) Perdew, J. P.; Wang, Y. Accurate and Simple Analytic Representation of the Electron-gas correlation-energy. *Phys. Rev. B: Condens. Matter Mater. Phys.* **1992**, *45*, 13244–13249.
- (30) Klimeš, J.; Bowler, D. R.; Michaelides, A. Chemical Accuracy for the Van Der Waals Density Functional. *J. Phys. Condens. Matter* **2010**, *22*, 022201.
- (31) Klimes, J.; Bowler, D. R.; Michaelides, A. Van Der Waals Density Functionals Applied to Solids. *Phys. Rev. B: Condens. Matter Mater. Phys.* **2011**, *83*, 195131–195143.
- (32) Mishin, Y.; Mehl, M. J.; Papaconstantopoulos, D. A.; Voter, A. F.; Kress, J. D. Structural Stability and Lattice Defects in Copper: Ab initio, Tight-binding, and Embedded-atom Calculations. *Phys. Rev. B: Condens. Matter Mater. Phys.* **2001**, *63*, 224106.
- (33) Monkhorst, H. J.; Pack, J. D. Special Points for Brillouin-Zone Integrations. *Phys. Rev. B: Solid State* **1976**, *13*, 5188–5192.
- (34) Henkelman, G.; Uberuaga, B. P.; Jónsson, H. A climbing image nudged elastic band method for finding saddle points and minimum energy paths. *J. Chem. Phys.* **2000**, *113*, 9901–9904.
- (35) Henkelman, G.; Jónsson, H. Improved tangent estimate in the nudged elastic band method for finding minimum energy paths and saddle points. *J. Chem. Phys.* **2000**, *113*, 9978–9985.
- (36) Sun, K.; Zhao, Y.; Su, H.-Y.; Li, W.-X. Force Reversed Method for Locating Transition States. *Theor. Chem. Acc.* **2012**, *131*, 1118–1127.
- (37) Nitoń, P.; Żywociński, A.; Fialkowski, M.; Holyst, R. A “nano-windmill” driven by a flux of water vapour: A comparison to the rotating ATPase. *Nanoscale* **2013**, *5*, 9732–9738.
- (38) Jansen, A. P. J. *An Introduction to Kinetic Monte Carlo Simulations of Surface Reactions*; Springer, 2012; p 856.
- (39) Filot, I. A. W.; van Santen, R. A.; Hensen, E. J. M. The optimally performing Fischer–Tropsch catalyst. *Angew. Chem., Int. Ed.* **2014**, *53*, 12746–12750.
- (40) Filot, I. A. W.; Broos, R. J. P.; van Rijn, J. P. M.; van Heugten, G. J. H.; van Santen, R. A.; Hensen, E. J. M. First-principles-based microkinetics simulations of synthesis gas conversion on a stepped rhodium surface. *ACS Catal.* **2015**, *5*, 5453–5467.
- (41) Campbell, C. T. Future directions and industrial perspectives micro- and macro-kinetics: their relationship in heterogeneous catalysis. *Top. Catal.* **1994**, *1*, 353–366.
- (42) Campbell, C. T. Finding the rate-determining step in a mechanism: comparing dedonder relations with the “Degree of Rate Control”. *J. Catal.* **2001**, *204*, 520–524.
- (43) Stegelmann, C.; Andreasen, A.; Campbell, C. T. Degree of rate control: How much the energies of intermediates and transition states control rates. *J. Am. Chem. Soc.* **2009**, *131*, 8077–8082.
- (44) Stegelmann, C.; Schiødt, N. C.; Campbell, C. T.; Stoltze, P. Microkinetic modeling of ethylene oxidation over silver. *J. Catal.* **2004**, *221*, 630–649.
- (45) Behrens, M.; Studt, F.; Kasatkin, I.; Kuhl, S.; Havecker, M.; Abild-Pedersen, F.; Zander, S.; Girgsdies, F.; Kurr, P.; Knief, B.-L.; et al. The Active Site of Methanol Synthesis over Cu/ZnO/Al₂O₃ Industrial Catalysts. *Science* **2012**, *336*, 893–897.
- (46) Gokhale, A. A.; Dumesic, J. A.; Mavrikakis, M. On The Mechanism of Low-Temperature Water Gas Shift Reaction on Copper. *J. Am. Chem. Soc.* **2008**, *130*, 1402–1414.
- (47) Tang, Q.-L.; Chen, Z.-X.; He, X. A Theoretical Study of The Water Gas Shift Reaction Mechanism on Cu(111) Model System. *Surf. Sci.* **2009**, *603*, 2138–2144.
- (48) Wang, G.-C.; Nakamura, J. Structure Sensitivity for Forward and Reverse Water-Gas Shift Reactions on Copper Surfaces: A DFT Study. *J. Phys. Chem. Lett.* **2010**, *1*, 3053–3057.
- (49) Russell, J. N., Jr.; Gates, S. M.; Yates, J. T., Jr. Reaction of Methanol with Cu(111) and Cu(111) + O(ads). *Surf. Sci.* **1985**, *163*, 516–540.
- (50) Boucher, M. B.; Marcinkowski, M. D.; Liriano, M. L.; Murphy, C. J.; Lewis, E. A.; Jewell, A. D.; Mattera, M. F. G.; Kyriakou, G.; Flytzani-Stephanopoulos, M.; Sykes, E. C. H. Molecular-Scale Perspective of Water-Catalyzed Methanol Dehydrogenation to Formaldehyde. *ACS Nano* **2013**, *7*, 6181–6187.
- (51) Zuo, Z.-J.; Wang, L.; Han, P.-D.; Huang, W. Insights into the Reaction Mechanisms of Methanol Decomposition, Methanol Oxidation and Steam Reforming of Methanol on Cu(111): A Density Functional Theory Study. *Int. J. Hydrogen Energy* **2014**, *39*, 1664–1679.
- (52) Greeley, J.; Mavrikakis, M. Methanol decomposition on Cu(111): A DFT study. *J. Catal.* **2002**, *208*, 291–300.
- (53) Chen, Z.-X.; Neyman, K. M.; Lim, K. H.; Rösch, N. CH₃O decomposition on PdZn(111), Pd(111), and Cu(111). A theoretical study. *Langmuir* **2004**, *20*, 8068–8077.
- (54) Sakong, S.; Groß, A. Density Functional Theory Study of The Partial Oxidation of Methanol on Copper Surfaces. *J. Catal.* **2005**, *231*, 420–429.
- (55) Liu, Y.; Hayakawa, T.; Suzuki, K.; Hamakawa, S.; Tsunoda, T.; Ishii, T.; Kumagai, M. Highly active copper/ceria catalysts for steam reforming of methanol. *Appl. Catal., A* **2002**, *223*, 137–145.
- (56) Wang, G.; Morikawa, Y.; Matsumoto, T.; Nakamura, J. Why is Formate Synthesis Insensitive to Copper Surface Structures? *J. Phys. Chem. B* **2006**, *110*, 9–11.
- (57) Nakamura, I.; Nakano, H.; Fujitani, T.; Uchijima, T.; Nakamura, J. Synthesis and Decomposition of Formate on Cu(111) and Cu(110) Surfaces: Structure Sensitivity. *J. Vac. Sci. Technol., A* **1999**, *17*, 1592–1595.
- (58) Nakano, H.; Nakamura, I.; Fujitani, T.; Nakamura, J. Structure-dependent Dynamics for Synthesis and Decomposition of Formate Species over Cu(111) and Cu(110) Model Catalysts. *J. Phys. Chem. B* **2001**, *105*, 1355–1365.
- (59) Quan, J.; Kondo, T.; Wang, G.; Nakamura, J. Energy Transfer Dynamics of Formate Decomposition on Cu(110). *Angew. Chem., Int. Ed.* **2017**, *56*, 3496–3500.
- (60) Rameshan, C.; Stadlmayr, W.; Penner, S.; Lorenz, H.; Memmel, N.; Hävecker, M.; Blume, R.; Teschner, D.; Rocha, T.; Zemlyanov, D.; et al. Hydrogen Production by Methanol Steam Reforming on Copper Boosted by Zinc-Assisted Water Activation. *Angew. Chem., Int. Ed.* **2012**, *51*, 3002–3006.